Microstructure and Corrosion Behaviour of ZnNiP Thin Film Alloys in Deep Eutectic Solvent Ionic Liquids

ELENA IONELA NEACŞU[1], VIRGIL CONSTANTIN[1]*, MARIAN BURADA[2], CRISTINA DONATH[1], VASILE SOARE[2], ANA-MARIA POPESCU[1]*

[1]Ilie Murgulescu Institute of Physical Chemistry of the Romanian Academy, 202 Splaiul Independentei, 060021, Bucharest, Romania
[2]National R&D Institute of Nonferous and Rare metals-IMNR, 102 Biruintei Blvd., 077145, Pantelimon, Ilfov, Romania

Ternary ZnNiP alloy thin films were electroless deposited from aqueous chloride electrolytes on mild steel foils. The films were characterized by scanning electron microscopy (SEM) and dispersive X-ray microanalysis (EDAX). The corrosion behaviour of ZnNiP thin films alloys was investigated in two deep eutectic solvent ionic liquids (DES) with different chemical structure at 353K and compared with corrosion in 3.5% NaCl aqueous solution at 273K. The films were characterized by X-ray photoelectron spectroscopy (XPS) to determine their chemical composition in the initial stage and after corrosion. The nature of corrosion morfology has been investigated by and electron microscopy and XPS. The value of the lowest corrosion protection efficiency was of 48.14% and the highest value was of 77.96%. The results confirmed the high corrosion resistance of ZnNiP alloy plated sheet in all ionic liquids systems tested and the results were corelated with corrosion data in aqueous solution. The passive layer consists of Zn and Ni oxides but also of the chemical compounds of nitrogen which were formed on the surface of the ZnNiP thin films during the corrosion process.

Keywords: ZnNiP thin films, Microstructure, Ionic liquids, Corrosion resistance, XPS

ZnNiP alloys are important in applications for anticorrosive protection of steel parts for energy systems, transportation, chemical equipment production, metallic constructions, etc. Zinc exhibits a very negative electrode standard potential (E_0=-0.76 V, measured *vs*. hydrogen normal electrode), thus being capable of acting as a sacrificial coating for plate. Ternary ZnNiP alloys were of special interest because of the corrosion resistance enhanced capability brought by an addition of 1-5% P in ZnNi alloys. Anticorrosive ZnNiP thin films depositions can be performed both electrochemically as well as chemical plating (electroless deposition), [1-10]. The mechanism of incorporating phosphorus in the alloy is complex and it is based both on direct electrochemical reactions of Ni^{2+} and Zn^{2+} reduction [11-13] and indirect electrochemical reactions, as $H_2PO_2^-$ disproportionation reaction resulting in phosphorous incorporation in the cathodic deposited alloy. Many studies were done on the corrosion of these ternary alloys in aqueous media [14,15]. Ionic liquids (ILs) have been widely investigated for a variety of applications: the use as solvents for chemical synthesis media, for electrodeposition of metals electrolyte, for electrochemical devices and fluids for thermal storage [16]. As long as we know there are studies on obtaining ZnNiP from IL [17], but no studies on the corrosion behaviour of these ternary alloys in these media were reported in literature. The present study describes the experimental works performed for electroless obtaining of ZnNiP thin films on steel substrate from alkaline chloride aqueous solutions and the corrosion behaviour of these alloys in deep eutectic solvent ILs.

Experimental part
Materials

ZnNiP thin films were electroless deposited [samples ZnNiP(1), ZnNiP(2) and ZnNiP(3)] on low carbon steel substrate (composition $Fe_{99.49}$-$C_{0.0043}$-$Si_{0.044}$-$Mn_{0.41}$-$Ni_{0.011}$). The carbon steel substrate was first polished with SiC paper from grade O100 to grade O400, and was subjected to a special surface finishing before deposition: cleaning in acetone, cleaning in an alkaline solution for 10 min at 353K, cleaning in 10 vol.% H_2SO_4 solutions, for 30 s, at 273 K, electrocleaning in an alkaline solution for 20-25 min according to ASTM G1-03 (the current density was 10 mA cm^{-2}) [18]; after each step, the specimens were rinsed with deionized water. The thin film alloys preparation conditions are presented in Table 1.

*email: virgilconstantin@yahoo.com, popescuamj@yahoo.com

Table 1
CHEMICAL COMPOSITION AND CONDITIONS OF THE AQUEOUS DEPOSITION BATH

Samples	Chemical composition g/l					pH	T
	$NiCl_2$ $\times 6H_2O$	$ZnCl_2$	NaH_2PO_2 $\times H_2O$	$C_6Na_3H_5O_7$ $\times 5½H_2O$ (Sodium citrate)	NH_4Cl		(K)
ZnNiP(1)	47	10	45	4	26	9.5	358
ZnNiP(2)	50	10	50	10	100	9.5	343
ZnNiP(3)	135	62	20	21	22	9.0	303

The deposition time was kept constant at 120 min. All solutions were prepared with analytical grade reagents (obtained from Merck, USA) dissolved in triply distilled water. After the electroless deposition, the samples were washed with distilled water and dried with hot air. All experiments were carried out in duplicate and the ability to reproduce these sample was found satisfactory. Film thickness is determined using the equation: h=G/2ρS, where h is the film thickness (μ), G is the weight of the deposited alloy (g), ρ is the density of Zn-Ni-P alloy (≈ 8.5 g cm^{-3}) and S is the steel sample surface area (4 cm^2).

Surface morphology and chemical composition

The elemental distribution and surface morphology of deposits were examined using EDAX integrated with a scanning electron microscope (SEM) Philips XL-30 .To ensure accuracy, EDAX analysis was done at several points on the surface of the substrate. The accuracy of the measurements for the equipment used was rated as ±0.1 wt.%.

XPS analysis was performed before and after corrosion in order to know the morphology and surface composition of the studied samples. XPS measurement of the obtained thin films was carried out on a Quantera SXM equipment, with a base pressure in the analysis chamber of 10^{-9} Torr. The X-ray source was Al-Kα radiation (1.4866 keV, monochromatized), and the overall energy resolution is estimated at 0.65 eV by the full width at half maximum (FWHM) of the Au4f$_{7/2}$ line. In order to take into account the charging effect on the measured binding energies (BE), the spectra were calibrated using the C1s line (BE=284.8 eV, C–C (CH)n bondings) of the adsorbed hydrocarbon on the sample surface [19]. XPS data base[20,21] was used for identifying the deconvoluted peaks. The sensitivity of the XPS method is in the range of 10^{-3}–10^{-4} of a monolayer (ppb), so it is expected to have some differences from EDAX results. Quantitative analysis (relative concentrations) has estimated in the range of ±10%, while the accuracy for BE assignments was ±0.2 eV.

Corrosion test

Corrosion behavior of the ZnNiP thin film coatings was evaluated through potentiodynamic polarization tests using a PARSTAT 2273 potentiostat/galvanostat with a "Power Corr'' software. The polarization tests were conducted in two systems of deep eutectic solvent (DES) ILs based on choline chloride [(2-hydroxyethyl) trimethylammonium chloride]. All reagents (Choline chloride (ChCl, Sigma Aldrich >99%), urea (Sigma Aldrich >99) and ethylene glycol (Fluka > 99.5%) were used as purchased without recrystallization or drying, in order to simulate a more appropriate technological process for future industrial use. Popular names of DESs that are used throughout this work are Reline200 and Etaline100. Both are formed by mixing and heating ChCl with urea or ethylene glycol in a molar ratio corresponding to binary eutectic [respectively ChCl-urea (1:2 molar ratio) , for sample ZNP(1), ZNP(2) and ChCl-ethylene glycol (1:1M), for sample ZNP(3)] at 353 K until homogenous and color less liquid was formed. The corrosion experiments were catrried aut in both Reline200.and Etaline100 aerated solutions at 353 K. The obtained results were compared with the results obtained for corrosion resistance of these samples in 3.5 wt.% NaCl aqueous solution. A three electrode configuration assembed in a thermostatic glass cell was used. The specimen with an exposed area of 1 cm^2 was used as working electrode, glassy carbon (GC) as counter electrode and an Ag wire (Johnson Mathew) as a quasi reference electrode. For the experiments in 3.5 wt.% NaCl the SCE reference electrode was used. The cell assembly was located at a Faraday cage to prevent electrical interferences. The samples were immersed in the electrolyte before the tests started and were allowed to reach equilibrium, which usually took around 20 min. Linear polarization curves were obtained by sweeping the electrode potential in the range of ±20 mV *vs.* open-circuit potential (OCP) starting from cathodic area, after a constant value of OCP was achieved (up to 30 min) [22]. Also, Tafel polarization experiments were performed with a constant scan rate of 0.166 mVs^{-1}, while the potential was being shifted within ±250 mV *versus* E$_{OCP}$ [23,24]. Cathodic and anodic polarization was performed independently.

Results and discussions

Surface morphology and elemental analysis of the ZnNiP thin film alloys

The obtained measured thickness of the studied samples was: 15 μm for ZnNiP(1), 10 μm for ZnNiP(2) and 32 μm for ZnNiP(3). The adhesion of coating films to steel substrate was determined by applying and removing pressure-sensitive tape over cuts made in the film in accordance with ASTM D3359-09e2 [25]. The obtained results were: class 4B for ZnNiP(1), class 3B for ZnNiP(2) and class 1B for ZnNiP(3). The cross section microstructures of these samples are presented in Figure 1.

The morphology of the films is show in Figure 2, showing a uniform, homogenous and non porous deposit. The SEM images illustrate a "cauliflower" point-shaped spear specimen for the sample ZnNiP(1), with very large structures for the sample ZnNip(2) and a small, granular and multi-layered hollow structure for the sample ZnNiP(3).

For all samples on the EDAX spectra we have found the main constituents of the respective alloy to be Zn, Ni, P. Also, in all samples was found Fe (from the support on which the alloy was deposited) which means that the formed ZnNiP film is very thin. With regard to the ZnNiP(3) sample, it also shows an O content, which shows that the coverage is not very pure. We will demonstrate later that EDAX data are well related with XPS data.
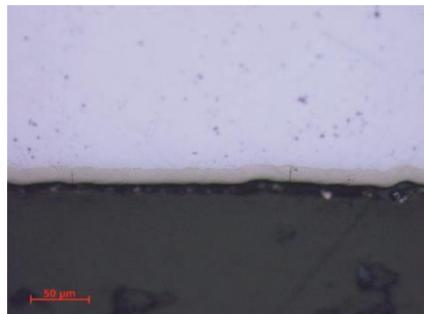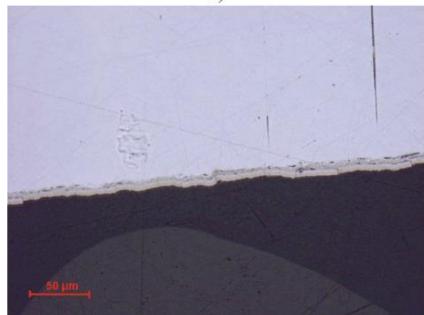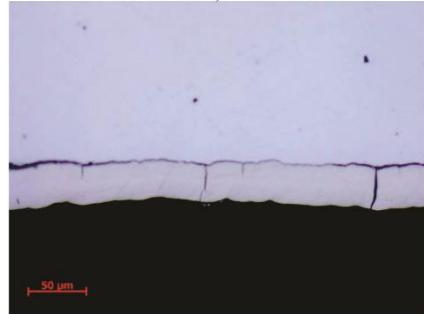
Fig.1 Microstructures of ZnNiP samples deposited electrolessly in chloride aqueous medium: a) ZnNiP(1), b) ZnNiP(2), c) ZnNiP(3)
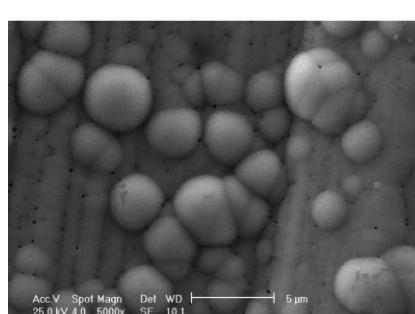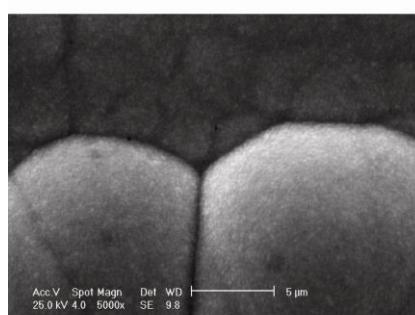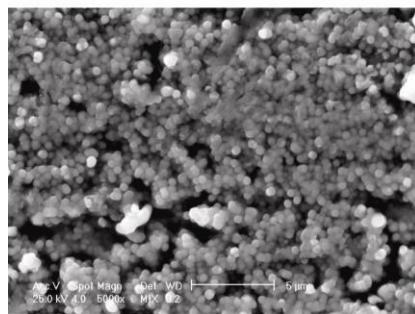
Fig. 2 The surface morphology (SEM images and EDAX spectra) of the ZnNiP thin films deposited on the steel substrate for the samples: a) ZnNiP(1), b) ZnNiP(2) and c)zNnIp(3)

Corrosion properties determined by potentiodynamic polarization

Comparative potentiodynamic polarization studies for uncoated carbon steel and carbon steel coated with ZnNiP alloy were carried out in order to evaluate the corrosion rate and chemical resistance in two systems of ILs [ChCl-urea (1:2 molar ratio) and ChCl-ethylene glycol (1:1 molar ratio)]. The open circuit potential (OCP) was evaluated for quantitative evaluation of the corrosion process. Linear polarization curves (not shown) and Tafel potentiodynamic polarization curves (Figure 3) were plotted as specific electrochemical procedure, which permitted the establishing of

the polarization resistance (R_p), corrosion potential (E_{corr}), corrosion current (i_{cor}), corrosion rate (CR) and protection efficiency (PE) [26,27].
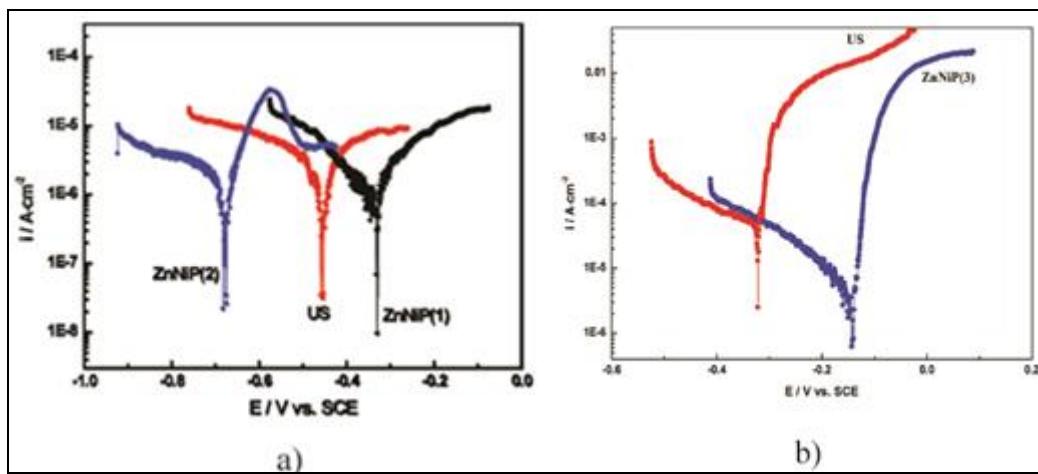
Fig. 3. Tafel plots for steel substrate (US) and ZnNiP(1, 2) in Reline200 (a) and ZnNiP(3) in Etaline100 (b)

The corrosion parameters obtained are presented in Table 2. For comparison of the results obtained in Ils and aqueous media, the same samples were also subjected to corrosion process in 3.5 wt.% NaCl (Table 3). For a given electrolyte solution, the OCP is dependent on the characteristics of resulted oxide, such as oxide thickness, chemical composition, electrical conductivity, structure, etc. At the initial time of immersion in Reline 200 environment the studied alloys present OCP potential values varying from -0.538V for uncoated steel (US) sample to -0.381 V for ZnNiP(1) and -0.693V for ZnNiP(2) sample, while for the immersion in Ethaline100 the OCP values were -0.295V for steel sample and -0.186V for ZnNiP(3) sample. Most rapid evolution of OCP potential occurs during the first 7-10 minutes of immersion, while further potential evolution becomes slower and OCP values do not change significantly, having a slow monotonous shift towards more positive values. The values of OCP for the studied ZnNiP alloys depend strongly of the zinc content in the alloy, but all OCP values of the studied ZnNiP samples in the two ILs exhibited more positive potentials than for carbon steel substrate (US). The time evolution of OCP indicates that the ZnNiP film is thin and consequently becomes vulnerable toward penetration of Cl⁻ ions. Also, we noticed slight oscillations of OCP in time. We assumed that these OCP oscillations may result from chemical interactions between chloride ions and the structured passive film. As in all samples the nickel content is higher than 73 wt.%, this behaviour may be considered as depending strongly on zinc and phosphorous content in the alloy.

Analyzing the data in Table 2 we can observed that the unprotected steel (US) sample has OCP potentials more positive in ionic liquids compared to aqueous solution, having in ChCl-ethylene glycol an the most positive value.

Table 2
THE CORROSION PARAMETERS MEASURED AND CALCULATED FOR THE STEEL SUBSTRATE (US)
AND THE STUDIED ZnNiP SAMPLES IN RELINE 200 AND ETHALINE 100 AT 353 K

Sample	E_{OCP} (V)	R_p (Ωcm^2)	E_{corr} (V)	i_{corr} ($A \cdot cm^{-2}$)	CR ($mm \cdot y^{-1}$)	PE (%)
US/Reline200	-0.512	166.135	-0.453	$2.903 \cdot 10^{-8}$	0.0217	0
ZnNiP(1)	-0.326	3219.15	-0.325	$8.931 \cdot 10^{-9}$	0.0048	77.96
ZnNiP(2)	-0.674	2273.83	-0.677	$2.427 \cdot 10^{-8}$	0.0081	62.72
US/Etaline100	-0.274	-	-0.318	$9.435 \cdot 10^{-6}$	0.0108	0
ZnNiP(3)	-0.162	-	-0.450	$6.441 \cdot 10^{-8}$	0.0056	48.14

E_{OCP} = open potential (rest potential); R_p = polarization resistance; E_{corr} = corrosion potential;
i_{corr} = corrosion current density; CR = corrosion rate; PE(%) = protection efficiency

Table 3
THE CORROSION PARAMETERS CALCULATED FOR THE ZnNiP SAMPLES AND FOR THE
UNPROTECTED STEEL SUPORT (US) IN 3.5% NaCl AQUEOUS SOLUTION AT 298 K

Sample	E_{OCP} (V)	E_{corr} (V)	i_{corr} ($A \cdot cm^{-2}$)	CR ($mm \cdot y^{-1}$)	PE (%)
US/NaCl	-0.54	-0.71	$8.96 \cdot 10^{-6}$	0.2104	-
ZnNiP(1)	-0.51	-0.74	$2.72 \cdot 10^{-6}$	0.0639	69.63
ZnNiP(2)	-0.53	-0.37	$17.72 \cdot 10^{-6}$	0.1823	13.35

E_{OCP}=rest potential; E_{corr}=corrosion potential; i_{corr}=corrosion current density;
CR=corrosion rate; PE=protection efficiency

As regarding the studied alloy samples the ZnNiP(2) which has a more negative E_{OCP} in Reline200 compared to that of US, this can suggest that ZnNiP(2) sample could function as a sacrificial layer for steel. From the evolution of the Tafel curves it is clear that the samples have the same aspect as the sample US, *i.e.* they show cathodic protection with anodic polarization, but have more positive corrosion potential [ZnNiP(1) and ZnNiP(3)] or more negative [ZnNiP(2)] with respect of the support steel. The evolution of corrosion currents also indicates the anticorrosive protection capacity, due to lower values than that for US, so the covered samples will have a corrosion protection capacity. By evaluating the corrosion behavior of ZnNiP in Reline200 (ChCl-Urea), we have found that the ZnNiP(1) sample has the lowest corrosion current extrapolated from the Tafel curves and implicitly the lowest corrosion rate. This sample also shows the highest polarization resistance calculated from the linear polarization curves. At the same time it is observed that the samples in the study have of lower corrosion current density in the ILs than in the aqueous solution, which is in line with the literature data regarding the alloy corrosion in ILs [28]. It should also be added that the ZnNiP(2) sample, although having a lower corrosion rate than that of the ZnNiP(1) sample, it shows a strong passivation process and even anodic transpassivation (Figure 3a), which suggest that this sample even worked as layer of sacrifice, producing steel protection by passivation. We can link this behavior to sample structure (Figure 2) and conclude that ZnNiP(1) sample with medium and homogeneous globular structures is more resistant to corrosion than that with very large globular structures, ZnNiP(2). With regard to the ZnNiP(3) sample, its structure with small coarse grains and many holes as well as with the presence of oxygen, favors the appearance of corrosion centers and thus explains the low corrosion resistance of this sample in both aqueous and ionic solutions. With respect to the ZnNiP(3) sample whose corrosion was studied in Etaline 100, it was found to have the most positively OCP potential (-0.162 V). Considering that in a given corrosive environment an electrode with a more noble OCP being more thermodynamically stable than a less noble electrode, we can conclude that the stability of the ZnNiP alloy is better in ChCl-EG than in ChCl-Urea. The corrosion currents obtained in this study are in good agreement with the values obtained in ionic liquids in general, *i.e.* samples have very small currents [29]. Due to the complexity of the ionic fluid structure, the cathodic processes which can occur on the surfaces of metallic materials are very difficult to predict as shown by the potential fluctuations in the curves of Figure 3. The corrosion sequence of ZnNiP samples in ionic liquids studied is Etaline100 > Reline 200. The passivation tendency of samples in Reline 200 may be due to the presence of urea. From the corrosion sequence we can conclude that the presence in ethylene glycol (1,2 ethanediol) is more damaging compared to urea due to the presence of OH groups. The corroded surface was observed visually and micrographically for the identification of formation of any white/red rust on the coating. Literature show that when Zn-Ni alloy coatings are exposed to salt solutions, zinc hydroxide is found to form as corrosion product [30]. This product is known as "white rust" which bears the indication of corrosion. The same phenomenon we noticed when ZnNiP is exposed to salt solution.

The morpho-structural characterization by metallographic and visual microscopy (Figures 4 and 5) revealed structures with moderate deformation and low adherence, structures that are responsible for the behavior observed in electrochemical testing.
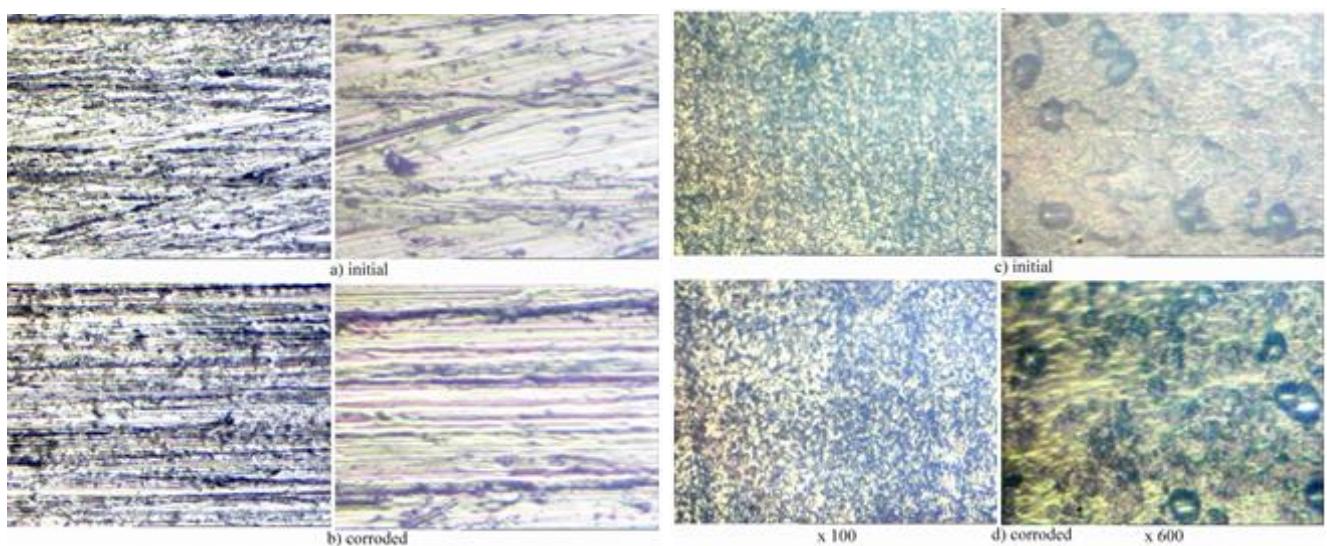
Fig. 4. Metallographic micrography with different magnifications for the samples ZnNiP(1) (a, b) and ZnNiP(2) (c, d) before and after corrosion in Reline200 at 353 K after 240 min
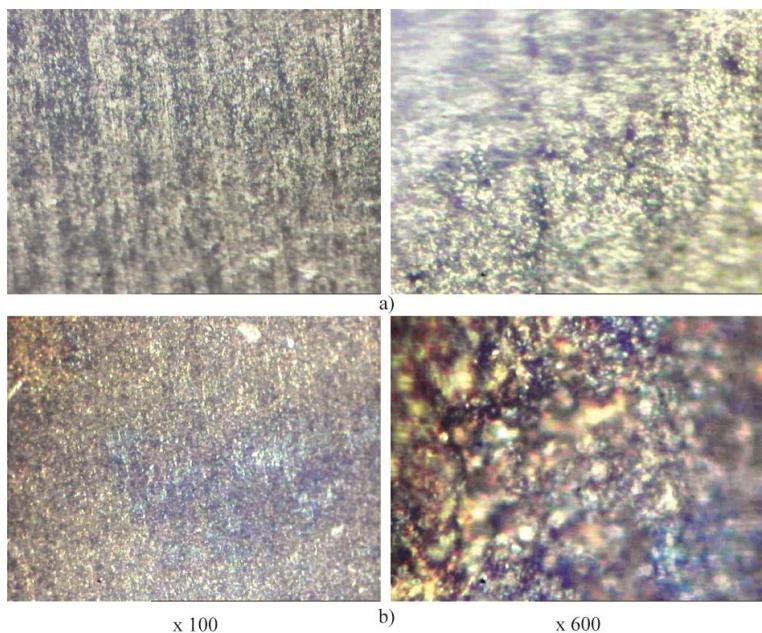
Fig. 5. Metallographic micrography with different magnifications for the sample ZnNiP(3) before (a) and after (b) corrosion in Ethaline 100 at 353 K after 240 min

Surface chemical composition before and after corrosion test determined by XPS

XPS analysis was used to determine the chemical states of the elements present on the surface of the Zn-Ni-P thin film alloys deposited on steel substrate before and after the corrosion process. Survey (wide scan) XPS spectra were recorded to detect all the elements present on the surface (<10 nm). High resolution spectra were collected to find out the chemical bonding of the detected elements and for quantitative analysis, as well. Figure 6 shows the comparison of XPS spectra with the binding energies (BE) in the range of 0-1200 eV for the studied samples before and after corrosion in the studied ionic liquids at 353K for 240min. From the XPS spectra we can state the following: in all samples studied (regardless the ionic liquids used) the presence of Zn2p peak, ZnLMM Auger peak, Ni2p and P2p peaks are observed, in addition to the main transitions O1s, C1s and OKLL, in different proportions, which can be confirmed by both the high resolution spectra and the respective concentrations (Table 4). After corrosion, a small characteristic peak appears also for N1s. The binding energies from Table 5 are in concordance with Handbook of X-ray photoelectron spectroscopy [31] and show peaks for the existence of ZnO, NiO/Ni_2O_3, P^0/P organic and N in organic matrix.

Also, the oxygen peaks are composed from two contributions representing O^{2-} and OH^-, a tiny amount of water for the polarized samples.The carbon detected on the surface comes from two sources: the surface is contaminated with unavoidable carbon from CO_2 and hydrocarbon adsorbed on the outermost layer from ambient atmosphere; another reason is the presence of an aromatic compound ($C_6Na_3H_5O_7 \times 5\frac{1}{2}H_2O$/sodium citrate) used in the bath of electroless deposition.

The ZnNiP(3) sample has an approximate unitary Zn/Ni ratio, suggesting that it might be less good in terms of corrosion resistance (already proven by the corrosion test).
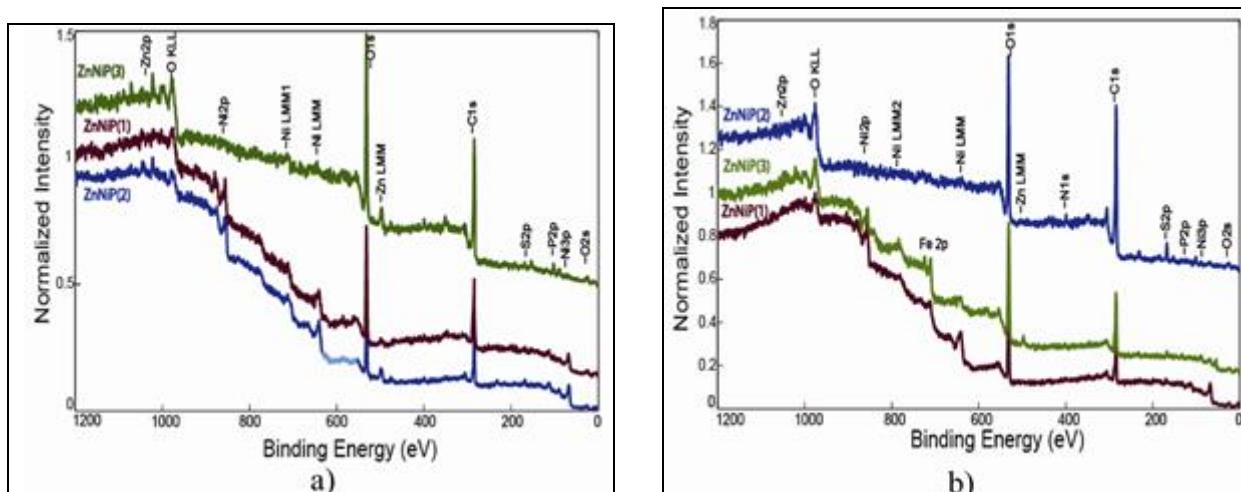
Fig. 6. XPS survey spectra for all samples ZnNiP(1), ZnNiP(2) and ZnNiP(3) before (a) and after (b) corrosion at 353 K and 240 min

Table 4
EXPERIMENTAL QUANTITATIVE XPS VALUES DETERMINED FOR THE INITIAL AND
CORRODED ZnNiP COATING SAMPLES IN DESs, FOR 240 min AT 343K

Element composition (wt.%)						
Samples	DES	Zn	Ni	P	Fe	N
ZnNiP(1) initial	Reline	2.85	92.35	4.80	-	-
ZnNiP(1) corroded		1.04	79.20	4.46	2.27	13.03
ZnNiP(2) initial	Reline	13.22	85.31	1.47	-	-
ZnNiP(2) corroded		10.91	75.13	0.81	4.49	8.66
ZnNiP(3) initial	Ethaline	32.55	60.07	7.38	-	-
ZnNiP(3) corroded		20.50	56.17	4.53	6.80	12.0

Table 5
SUMMARY OF BINDING ENERGIES FOR THE INITIAL AND CORRODED SAMPLES

Binding Energy (eV)									
Samples	Stage	DES	NiO 2p$_{3/2,1/2}$	Ni$_2$O$_3$ 2p$_{3/2,1/2}$	Ni (satellites)	P 2p	Zn 2p$_{3/2}$	Zn LMM	N 1s
ZnNiP(1)	initial	Reline	853.4	856.1	858.7	130.1	1022.2	497.5	-
			870.1	873.2	876.7	133.6	-	-	-
	corroded		853.4	855.8	861.2	130.1	022.2	497.8	398.1
			870.1	875.0	880.1	134.0	-	-	399.4
ZnNiP(2)	initial	Reline	853.5	855.0	859.9	133.2	1022.0	498.3	-
			870.5	873.9	875.7	-	-	-	-
	corroded		853.4	-	859.9	-	1022.3	-	398.8
			870.5	-	875.4	-	-	-	400.5
ZnNiP(3)	initial	Ethaline	853.8	855.9	860.0	133.2	1022.1	497.9	-
			871.0	873.1	877.3	-	-	-	-
	corroded		853.8	856.0	861.2	133.5	1022.3	497.2	398.2
			871.1	875.2	880.1	-	-	-	400.3

Figure 7, presents the registered XPS spectra for all elements: Ni, Zn, Zn LMM, P and N in all studied samples before and after corrosion. After corrosion the surface chemistry of the all samples shows significant changes by appearance a little peak characteristic of Fe because the ZnNiP deposits are very thin. The analysis of Table 4 shows that the amount Fe sample is higher ZnNiP(3), this sample had the lowest resistance to corrosion than the other two samples ZnNiP(1) and ZnNiP(2).

Thus, we can notice that while P relative concentration are in good agreement, the Ni and Zn relative concentration are different suggesting the diffusion of Ni from the surface into the subsurface region accompanied by segregation of Zn from subsurface region toward the outermost layer of the film. All elements decrease in the all sample, which presents an increased resistance to the corrosion process.
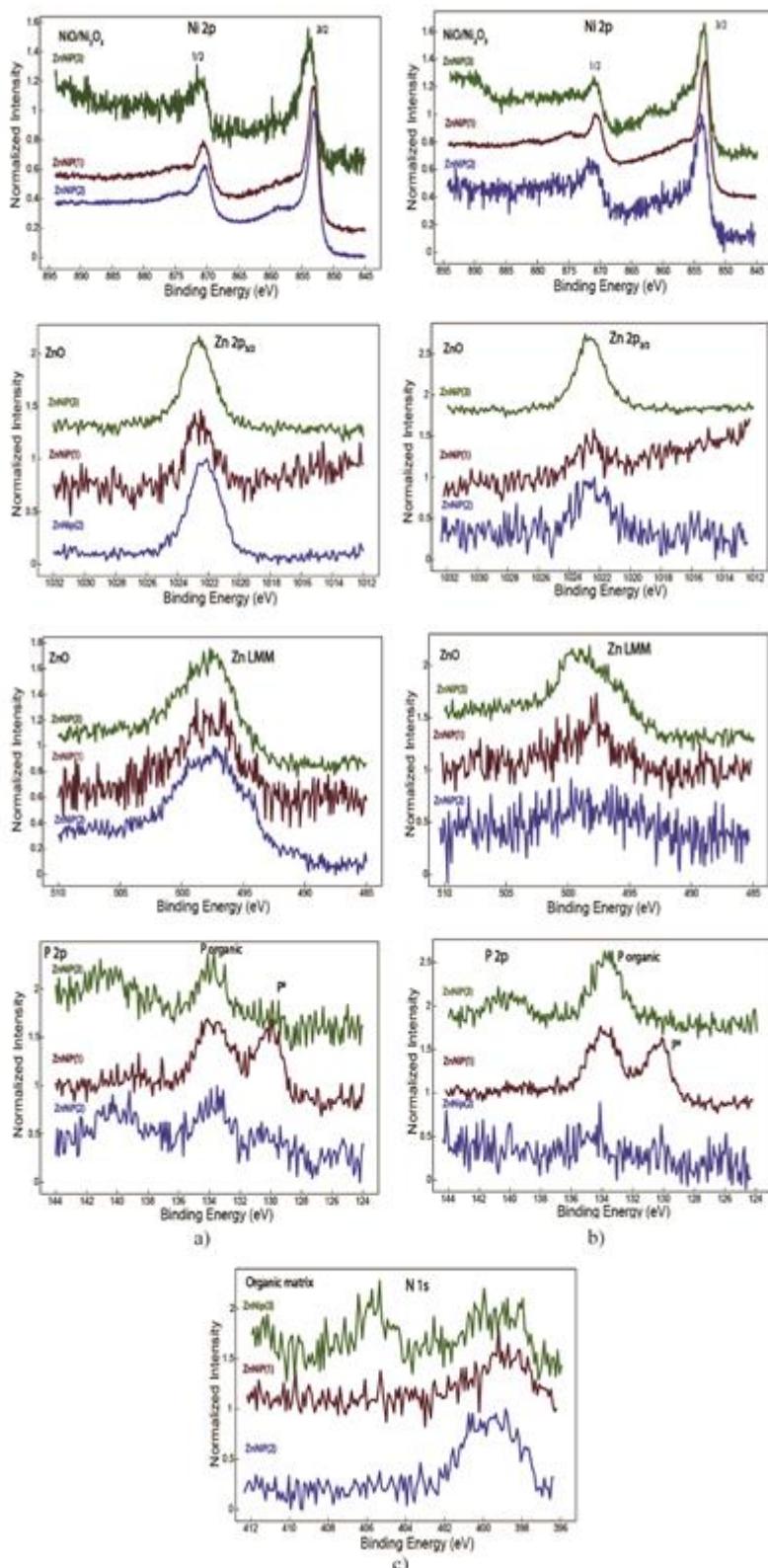
Fig. 7. XPS spectra for all ZnNiP samples before (a) and after corrosion (b, c) in the used ILs

Figure 8 presents the deconvoluted spectra for Zn (both 2p and LMM-transitions) before and after corrosion. Both spectra for the Zn $2p_{3/2}$ and Zn LMM indicated the presence of Zn^{2+} ion as ZnO in all the film studied. Because it is practically impossible to detect a chemical shift between Zn^0 and Zn^{2+} states in the photoelectron line $Zn2p_{3/2}$, we recorded also the Auger LMM transition. The BE values of ZnO characteristic energy were from 497.2 to 498.3 eV, which can be easily seen from Table 5. On the other hand, the specific BE values for metallic Zn are ranging from 495.1 to 495.9 eV. One can observe that only the Zn LMM Auger transition exhibits a chemical shift of ~2.5 eV to higher BE for Zn in its +2 oxidation state as compared with Zn^0. From the Auger LMM transition, it becomes clear that inclusion of Zn in the inital stage of ZnNiP electroless thin films is found to be in the +2 oxidation state as ZnO

(497.5 eV - 498.3 eV). For the corroded samples the corrosion products of ZnNiP alloy platted steel were found to consist of zinc compound ZnO (at 497.2 eV - 497.8 eV).

The detailed XPS spectra of nickel are presented in Figure 9. The deconvoluted spectra for the initial ZnNiP samples (Figure 9a), asociated to nickel show the existence of a mixture of Ni^{2+} and Ni^{3+} chemical states from the line profile (including satellites) and the position of the $Ni2p_{3/2}$ peak. The characteristic BE values of the $2p_{3/2}$ feature (853.4, 853.5, 853.8 eV); 856.1, 855.0, 855.9 eV), the band-like profile of the spectrum, as well as the presence of the associated satelittes at (857.7, 859.9, 860.0 eV) are the fingerprints of a mixture of NiO and Ni_2O_3. The relative concentrations of nickel in these two different chemical states are 40% Ni_2O_3 and 60% NiO. For all samples corroded we noticed that do not occur compositional changes, but only small decrease in the concentration (Table 4 and Fig.9b)
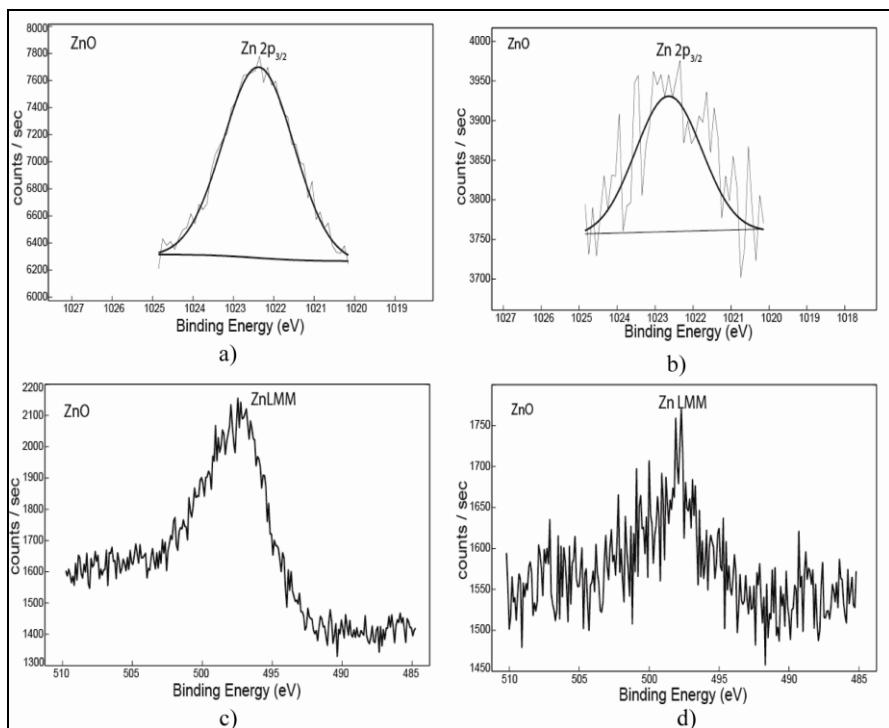
Fig. 8. The peak deconvolution of spectra of $Zn2p_{3/2}$ and Zn LMM Auger transition before (a,c) and after corrosion (b,d) in the used ILs
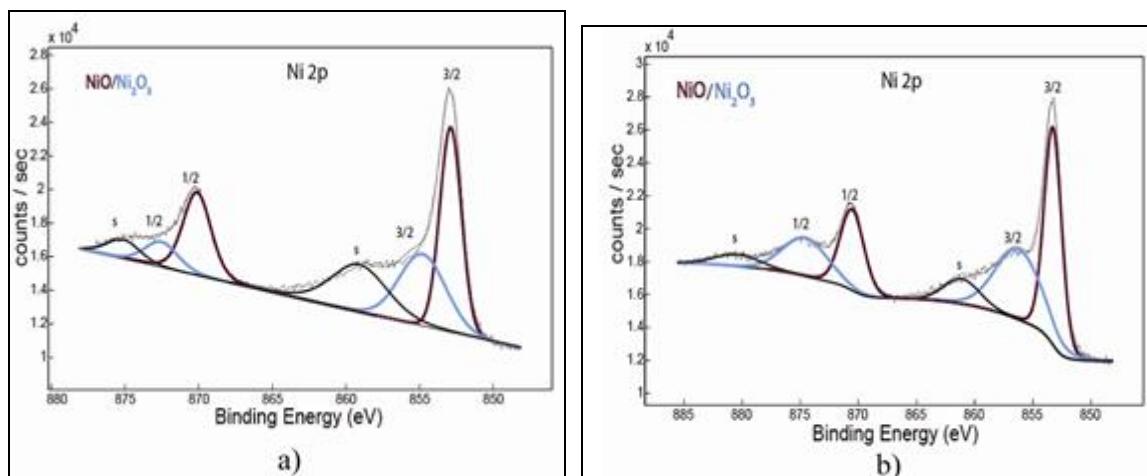
Fig. 9. The peak deconvolution of spectra of Ni2p before (a) and after corrosion (b) in the used ILs.

The detailed XPS spectra of phosphorus P2p (Figures 7 and 10) are very noisy in both initial and corroded states of the sample as a result of the tiny relative concentration of this element in the Zn-Ni-P thin films. The spectra show two different peaks for the initial and corroded sample ZnNiP(1) with a peak appeared at a binding energy of ~ 130.1-130.2 eV which is detected as elemental phosphorus (P^0). The phosphorus signal at the binding energy of 133.2 eV can be assigned to an organic combination of phosphorous ($P_{organic}$), especially in ZnNiP(2) and ZnNiP(3) samples, proving the excepted citrate complexes in the deposition bath.
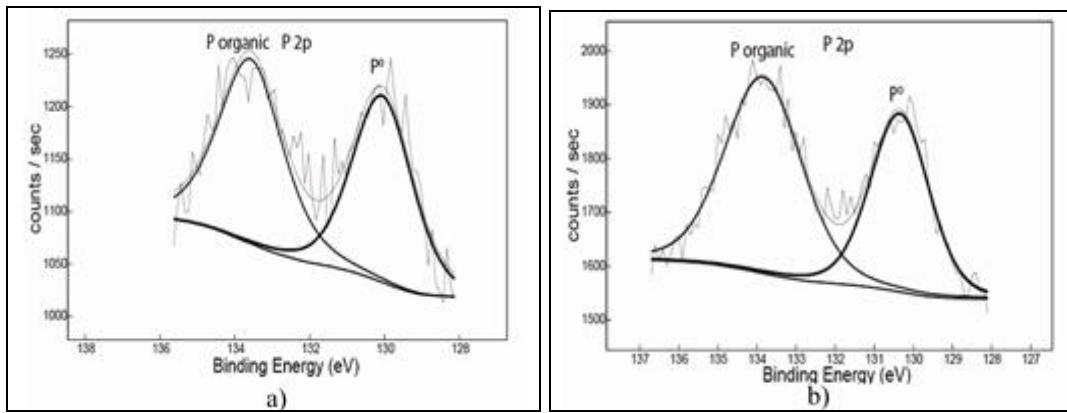
Fig. 10. The peak deconvolution of spectra of P2p before (a) and after corrosion (b) in the used ILs.

In the case of the all corroded samples it can be noted a signal given of nitrogen (Figures 6 and 7c). As can be seen in the detailed XPS spectrum for nitrogen (N1s), Figure 11 is very noisy as a result of the tiny relative concentration of this element. The first peak is attributed to the oxidation state N^{3-}(nitride). After deconvoluted spectrum it was found that the second peak is a part of an organic matrix, which may be derived from the ionic liquid used as the corrosion medium. The characteristic BE values of the N1s feature 398.1, 398.8, 398.2 eV (Table 5). Nitrogen is segregated to the alloy surface where it forms a relatively stable interstitial nitride phase. Thus we can conclude that the presence of N leads to anticorrosive protection for all three samples, by reducing the corrosion currents. This also correlates with the micrographs results.
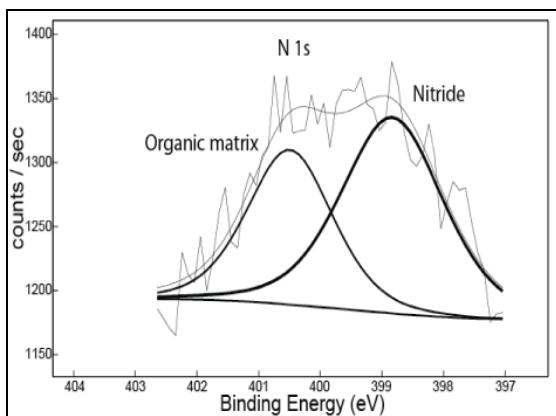
Fig. 11. The peak deconvolution of
of N1s in the used ILs

Conclusions

ZnNiP thin films were successfully prepared on low carbon steel substrate by electroless deposition from hypophosphite low alkali aqueous bath. The thin film is compact, uniform and has microcrystalline phases. EDAX elemental analysis confirmed the formation of ZnNiP coating with high Ni content. The XPS results demonstrated that the incorporation of Zn in the Ni-P electroless thin layer is possible using this electroless process. It also has been demonstrated that ZnNiP alloys show good corrosion resistance in choline chloride based eutectic ILs relative to aqueous sodium chloride solutions, although corrosion in this case occurred at a higher temperature (353 K) than that in the aqueous NaCl solution (298 K). Also taking into account the value of the corrosion rate of the control steel in the two ILs in the study, it was found that the ChCl-ethylene glycol (Ethaline100) is ultimately more corrosive than ChCl-urea (Reline200).

This good resistance to corrosion is given both by the passive layer of nickel oxides formed on the surface of ZnNiP thin films and by the incorporation of nitrogen into the passive layer structure, which reduced the corrosion current.

References
1. HOLBREY, J.D., SEDDON, K.R. Clean Prod. Proc., **1**, 1999, p. 223.
2. WELTON, T. Chem. Rev., **99**, 1999, p. 2071.
3. ENDRES, F. ChemPhysChem, **3**, 2002, p. 144.

4. LIN, Y.F., SUN, I.W. Electrochim. Acta, **44**, 1999, p. 2771.

5. POPESCU, A.M., DONATH, C., NEACSU, E.I., SOARE, V., CONSTANTIN, V. Rev. Chim.(Bucharest), **67**, no. 6, 2016, p. 1076.

6. TAKAHASHI, S., KOURA, N., KOHARA, S.,SABOUNGI, M.L.,CURTISS, L.A. Plasmas & Ions, **2**,1999, p. 91.

7. BRENNECKE, J.F., MAGIN E.J. AIChE J., **47**, 2001, p. 2384.

8. UE, M., TAKEDA, M., TORIUMI, A., KOMINATO, A., HAGIWARA, R., ITO, Y., J. Electrochem. Soc., **150**, 2003, p. A499.

9. BALDUCCI, A., BARDI, U., CAPORALI, S., MASTRAGOSTINO, M., SOAVI, F. Electrochem. Commun., **6**, 2004, p. 566.

10. MOENS, L., BLAKE, D.M., RUDNICKI, D.L., HALE, M.J. J. Sol. Energy. Eng, **125**, 2003, p. 112.

11. DURAIRAJAN, A., KRISHNIYER, A., HARAN, B.S., WHITE, R.E., POPOV, B.N. Corrosion, **56**, 2000, p. 283.

12. HUANG, Y.S., CUI, F.Z. Surf. Coat. Tech., **201**, 2007, p. 5416.

13. WANG, R., YE, W., MA, C., WANG, C. Mater. Character., **59**, 2008, p.108.

14. SRIVASTAVA, C., GHOSH, S.K., RAJAK, S., SAHU, A.K., TEWARI, R., KAIN V., DEY, G.K. Surf. Coat. Techn., **313**, 2017, p. 8.

15. REHIM, S.S.A.E., FOUAD, E.E., WAHAB, S.M.A.E., HASSAN, H.H. Electrochim. Acta, **41** 1996, p. 1413.

16. DURAIRAJAN, A., HARAN, B.S., WHITE, R.E., POPOV, B.N., J. Electrochem. Soc., **147**, 2000, p. 1781.

17. BOUANANI, M., CHERKAOUI, F., FRATESI, R., ROVENTI, G., BARUCCA, G.J. Appl. Electrochem., **29**, 1999, p. 637.

18. *** ASTM G1-03, Standard practice for preparing, cleaning, and evaluating corrosion test specimens, PA, ASTM International, 2011, https://doi.org/10.1520/G0001-03R11.

19. KANG, H.B., BAE, J.H., LEE, J.W., PARK, M.H., LEE, Y.C., YOON, J.W., JUNG, S.B., YANG, C.W. Scripta. Mater., **60**, 2009, p. 257.

20. MOULDER, J.F., STICKLE, W.F., SOBOL, P.E., BOMBEN, K.D., Handbook of X-ray photoelectron spectroscopy. CHASTAIN, J., KING JR R.C. (eds.). Minnesota, Physical Electronics Inc, 1995.

21. GROSVENOR, A.P., BIESINGER, M.C., SMART, R.S.C., MC INTYRE, N.S. Surf. Sci., **600**, 2006, p. 1771.

22. Yang, L., Li, J., Zheng, Y., Jiang, W., Zhang, M. J. Alloys Compd., **467**, 2009, p. 562.

23 REVIE, R.W. (ed.). Uhlig's Corrosion Handbook, 3-rd ed., John Wiley & Sons Inc, NJ, 2011.

24. Zhang ,W.X., He, J.G., Jiang, Z.H., Jiang, Q., Lian, J.S. Surf. Coat. Technol., **201** 2007, p. 4594.

25. ASTM D3359-09e2, Standard Test Methods for Measuring Adhesion by Tape Test,ASTM International, West Conshohocken, PA, 2009, https://doi.org/10.1520/D3359-09E02.

26. VEERARAGHAVAN, B., HARAN, B., KUMARAGURU, S.P., POPOV, B., J. Electrochem. Soc., **150**, 2003, p. B131.

27. REVIE R.W., UHLIG H.H. Corrosion and Corrosion Control. An Introduction to Corrosion Science and Engineering, fourth ed., John Wiley & Sons Inc., NJ, 2008.

28. PERISSI, I., BARDI, U., CAPORALI, S., LAVACCHI, A. Corros. Sci., **48**, 2006, p. 2349.

29 PERISSI, I., CAPORALI, S., FOSATTI, A., LAVACCHI, A. Corrosion resistance of metallic materials in ionic liquids.chapter 12 in: Advanced in Chemistry Reseach vol.6, Taylor JC, (ed.)., NOVA Science Publishers Inc, NY, 2011.

30. RAHMAN, M.J., SEN, S.R., MONIRUZZAMAN, M., SHOROWORDI, K.M., J. Mech. Eng. (Trans. of the Mech. Eng. Div., The Institution of Engineers, Bangladesh), **ME40**, 2009, p. 9.

31 LEE, H.L., FLYNN, N.T., X-ray photoelectron spectroscopy.chapter 11 in: Handbook of Applied Solid State Spectroscopy. VIJ, D. (ed.). MA, Springer, 2006.

───────────────